Thermopile power measurement for heat balance calorimetry

Callum M. Johnston, Bryan P. Ruddy, Poul M. F. Nielsen, Andrew J. Taberner

The University of Auckland
Auckland, New Zealand
callum.johnston@auckland.ac.nz

Abstract—**Very high resolution power sensors are required for measuring the rate of heat production (~10 µW) of small samples of heart muscle (rat cardiac trabeculae, ~2 mm long and ~200 µm diameter). In this paper, we examine the design criteria for thermopiles to maximize their signal-to-noise ratio for heat balance calorimetry. We found that those thermopiles with a high thermoelectric figure-of-merit (ZT) are the best for power measurements. An initial prototype with a resolution of 53 nW has been built.**

Keywords- Calorimetry, thermal variables measurement, thermal sensors, thermal noise

I. INTRODUCTION

Heat balance calorimeters are a special class of calorimeters for power measurement. These calorimeters measure the change in temperature of a flowing fluid to infer the rate of power output of a heat source [1], [2]. Heat balance calorimeters are often used in systems where the heat source is temperature-dependent because the fluid flow keeps the source at an approximately constant temperature [3].

Heat balance calorimeters are ideally suited for measuring the heat output of physiological tissue samples such as muscle fibers. In addition to regulating the tissue temperature, the fluid flow allows the tissue to be kept viable by supplying it with oxygen and nutrients, and by removing waste products [4]. However, for the tissue to remain viable, it must be sufficiently thin for diffusion to supply all of its parts with sufficient oxygen and nutrients [5], [6].

The Auckland Bioengineering Institute (ABI) has developed a heat balance calorimeter that measures the rate of heat production of a living cardiac muscle preparation. The muscle preparation is sufficiently small (~2 mm long and ~200 µm diameter) to allow sufficient oxygen to be supplied via diffusion [6]. The disadvantage of such small preparations is that they have correspondingly diminutive rate of heat production (~10 µW) at room temperature.

Fig. 1 shows a detail of the ABI calorimeter. The muscle preparation is held between two platinum hooks in the center of a 1 mm inner dimension square borosilicate glass capillary. The upstream hook is attached to a motor and the downstream hook is attached to a force transducer to allow control and measurement of the muscle length and force production.

Oxygenated Tyrode's fluid flows through the capillary tube past the muscle [7]. At a flow rate of 0.5 µl/s the heat output of
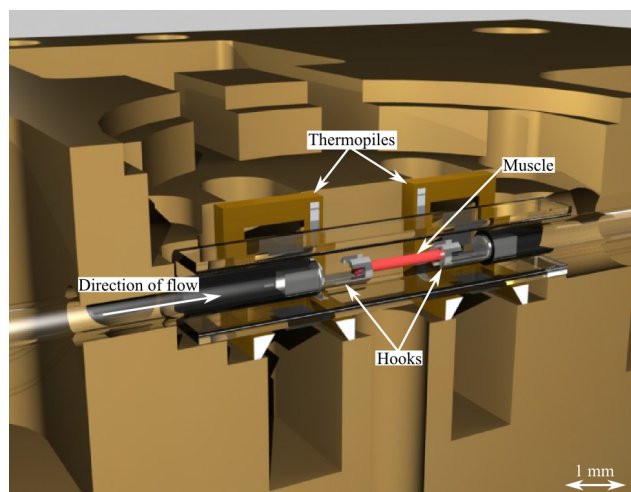
Figure 1. Calorimeter for measuring the rate of heat output and force production of rat cardiac trabeculae.

the muscle raises the fluid temperature by ~1.3 mK, which is sensed by an array of thermopiles upstream and downstream of the muscle. The ABI calorimeter has a signal-to-noise ratio (SNR) of 140, which is insufficient to adequately capture changes in the thermodynamics during some test protocols. Higher resolution power measurements should be possible through careful selection of the thermopile modules used for temperature measurement.

A number of groups have investigated the use of thermopiles for heat balance calorimetry [8]–[10]. These groups focused on creating thermopiles with high thermal resistances and high temperature sensitivities. A resolution of 50 nW over a 1 Hz bandwidth was obtained using these thermopiles [11]. The resolution typically was limited by environmental temperature fluctuations, therefore the thermal resistance and the sensitivity were maximized with no concern for the increased noise due to an increase in electrical resistance [8], [11]. However, the ABI calorimeter has been found to have sufficiently stable temperatures that Johnson noise is the limiting factor on the resolution [12]. The objective of this paper is to develop a holistic model of calorimeter performance incorporating both the sensitivity and the inherent noise of thermopiles, and to use it to evaluate possible transducers for a next-generation calorimeter.

II. Modeling

A. Analytical Model

A simple lumped-parameter analytical model was used to investigate how various thermopile parameters affect the SNR. This model examined the heat path between the fluid and the copper housing across the downstream thermopile as shown in fig. 2.

A steady-state model with adiabatic boundaries was created, with heat only permitted to flow through the thermopile and fluid outlet. There was assumed to be no heat conduction in the x direction except via the thermopile substrate, which was assumed to be a perfect conductor. The substrate's thermal conductivity was 20-fold higher than any of the other components in the system with the exception of the copper housing. The fluid temperature was assumed to be constant in y and z and the copper housing was taken to be a perfect heat sink. All temperatures are given relative to the housing, and the inlet fluid temperature is equal to that of the housing.

The temperature difference between the fluid and the substrate at any point may be found by performing a heat balance analysis on the infinitesimally thin section (in the x direction) of the fluid. The resulting temperature profile is given by

$$T_f(x) - T_s = (T_f(0) - T_s) exp\left(\frac{-x}{\dot{m}C_p X R_g}\right),$$

(1)

where T_f and T_s are the fluid and substrate temperature, respectively, x is the distance from the start of the thermopile, $\dot{m}$ is the fluid mass flow rate, C_p is the fluid specific heat capacity, X is the total length and R_g is the absolute thermal resistance of the glass. The rate of energy entering the fluid volume is equal to the rate of energy output of the muscle, i.e., $\dot{m}C_pT_f(0) = \dot{Q}$.

The substrate temperature may be found by considering a heat balance across the total fluid volume above the thermopile. Solving for the substrate temperature gives

$$T_s = \dot{Q}R_p\left(\frac{\varepsilon}{1 + \dot{m}C_pR_p\varepsilon}\right),$$

(2)

where R_p is the absolute thermal resistance of the pillars and

$$\varepsilon = 1 - exp\left(\frac{-1}{\dot{m}C_pR_g}\right).$$

(3)

ε is the heat exchanger effectiveness and reflects the efficiency of heat transfer between the fluid and the substrate if the substrate is assumed to be a heat sink, i.e. R_p is zero [13].

Given the model assumptions, the temperature difference across the pillars (dT) is equal to the substrate temperature. The dependence of dT on the absolute thermal resistance of the pillars and the glass is shown in fig. 3. The temperature difference is maximized by using a system with a high combined pillar thermal resistance and a low glass thermal resistance.

The temperature difference could be maximized by using a single thermocouple with extremely thin, extremely high pillars. The resulting sensor, however, would have a low sensitivity and a high resistance, thus suffering from high Johnson noise. It is therefore more useful to consider the SNR.

The signal may be estimated from multiplying the temperature difference by the number of thermocouples (n) and the Seebeck coefficient (S) of each thermocouple. The dominant noise source in thermocouples is typically Johnson noise [14]. Therefore, the SNR may be found by dividing the expected voltage difference by the Johnson noise, such that

$$\text{SNR} = \frac{nSdT}{\sqrt{4k_BTR_e\Delta f}},$$

(4)

where k_B is the Boltzmann constant, T is the absolute temperature, R_e is the electrical resistance and Δf is the measurement bandwidth.

Combining (2) and (4), as well as the electrical resistance as a function of the number of thermocouples, the ratio of pillar area (A_p) to height (Z_p) and the pillar's electrical resistivity (ρ) gives
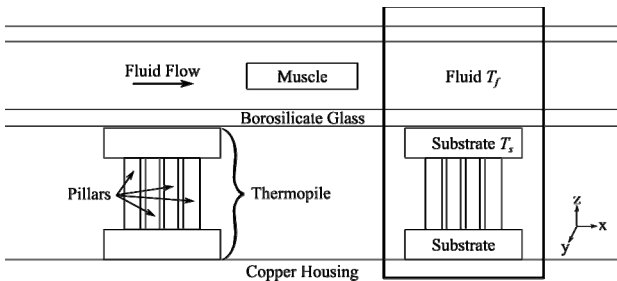
Figure 2. Schematic of the calorimeter system. The lumped parameter model examines the section of the calorimeter contained within the box.
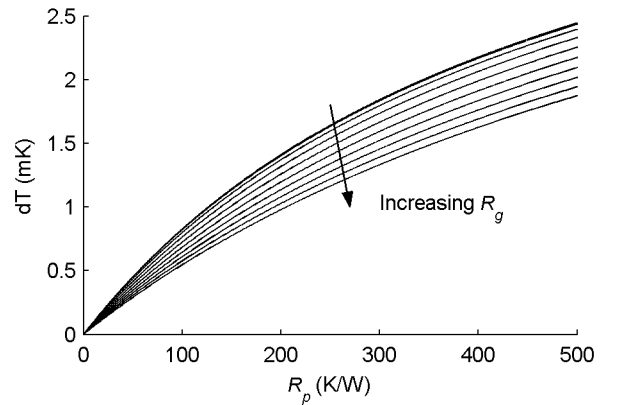
Figure 3. Predicted temperature difference across a thermopile depending upon the pillar thermal resistance (R_p) and the glass thermal resistance (R_g). R_g varies linearly between 0 K/W and 500 K/W. The temperature difference was calculated for fluid flow rate of 0.5 µl/s and a muscle heat output of 10 µW.

$$\text{SNR} = \frac{\dot{Q}S\sqrt{R_p}}{\sqrt{16k_B\kappa_p\rho\Delta fT}} \cdot \left[\frac{\varepsilon}{1+\dot{m}C_pR_p\varepsilon}\right], \quad (4)$$

where κ_p is the thermal conductivity of the pillars.

The dependence of the SNR on the number of pillars and their form factor was examined in fig. 4. The maximum SNR is independent of the pillar geometry.

The maxima occur at the same pillar thermal resistances. Therefore, there is an ideal thermal resistance for any combination of volumetric flow rate and specific heat capacity of the fluid. The thermal resistance at which the maximum occurs depends on R_g but the effect is minimal over a relatively wide range. R_g can be up to 30 % of R_p with only a 5 % change in the value of R_p at which the maximum SNR occurs. The dependence of the SNR on the product of the mass flow rate and the specific heat capacity for a range of pillar thermal resistances is shown in fig. 5.

Equation (4) can be rewritten as

$$\text{SNR} = \frac{\dot{Q}}{2} \cdot \frac{\sqrt{ZT}}{\sqrt{4k_B\Delta fT^2G_p}} \cdot \left[\frac{\varepsilon}{1+\dot{m}C_pR_p\varepsilon}\right], \quad (5)$$

where G_p is the thermal conductance of the pillar layer and ZT is the dimensionless thermoelectric figure-of-merit often used in temperature control literature [15]. Z is the ratio of the Seebeck coefficient squared to the product of the resistivity and the thermal conductivity, and is closely linked to the efficiency of thermoelectric devices. A more efficient thermoelectric material therefore will also be a better power sensor.

The denominator of the second term in (5) is the phonon noise, a result of the random movement of energy carriers between the sensor and its environment [16], [17]. The movement occurs even when the sensor is in equilibrium with the environment, thus reflecting the absolute limit on thermal power measurement.

A range of commercial thermopile modules were assessed using the analytical model. Table I lists the properties of the
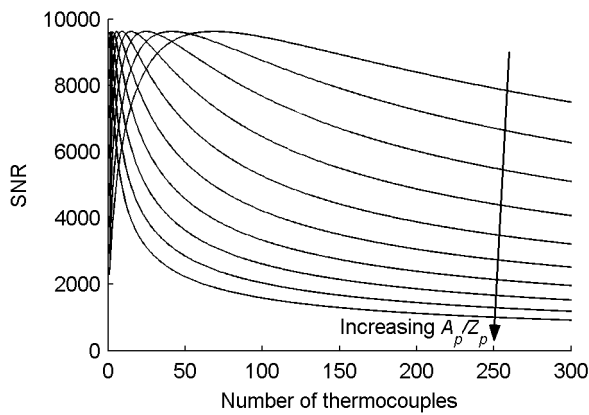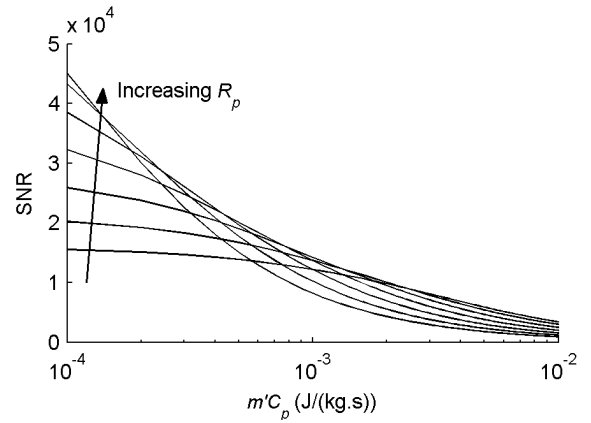

Figure 5. Predicted signal-to-noise ratio (SNR) for a range of thermal resistances of the pillars (R_p) and combinations of mass flow rate ($\dot{m}$) and specific heat capacity of the fluid (C_p). R_p varies logarithmically from $10^{2.5}$ K/W to 10^4 K/W. The thermal resistance of the glass was 100 K/W, the muscle heat output was 10 µW and the bandwidth was 5 Hz.

sensors, all of which use bismuth telluride thermocouples. Bismuth telluride is commonly used commercially as it has a high thermoelectric figure-of-merit ($ZT = 0.80$ at 25 °C). The SNR of these sensors is shown in fig. 6 as a function of the module length. The use of the same material means differences reflect changes in the sensors' absolute thermal resistances.

Fig. 6 indicates that those thermopiles with few, tall pillars will have the highest SNR. Thermopiles with this design are typically used for temperature control rather than temperature sensing. Consequently, sensors that are efficient temperature controllers are also those most suited for power measurement.

Figure 4. Predicted signal-to-noise ratio (SNR) across a thermopile depending upon the number of thermocouples and ratio of pillar area (A_p) to pillar height (Z_p). A_p/Z_p varies logarithmically from 10 nm to 1000 nm. The thermal resistance of the glass was 100 K/W, the fluid flow rate was 0.5 µl/s, the muscle heat output was 10 µW and the bandwidth was 5 Hz.
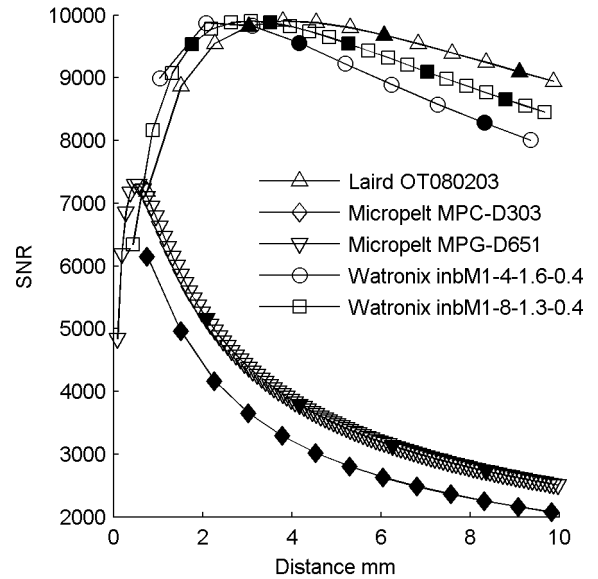

Figure 6. Predicted signal-to-noise ratio (SNR) depending on the thermopile design used and the total module length. Filled symbols indicate whole modules rather than partial modules. The fluid flow rate was 0.5 µl/s, the muscle heat output was 10 µW and the measurement bandwidth was 5 Hz.

Manufacturer	Module	Dimensions X (mm) • Y (mm) • Z (mm)			Number of Thermocouples	Resistance (Ω)
		Base	*Top*	*Pillar*		
Laird	OT080203	3.22 • 3.22 • 0.50	3.22 • 1.61 • 0.50	0.44 • 0.44 • 1.45	4	0.55
Micropelt	MPC-D303	0.83 • 2.42 • 0.53	0.83 • 1.18 • 0.53	0.69 • 0.07 • 0.04	4	0.3
	MPG-D651	2.50 • 3.35 • 0.53	2.50 • 2.50 • 0.53	0.04 • 0.04 • 0.04	286	185
Watronix	inbM1-4-1.6-1.3	4.18 • 3.34 • 0.50	4.18 • 2.18 • 0.50	0.70 • 0.70 • 1.65	4	0.39
	inbM1-8-1.3-0.4	2.04 • 3.22 • 0.50	2.04 • 2.04 • 0.50	0.26 • 0.26 • 1.35	8	2.97

B. Finite Element Model

The analytical model makes a number of simplifying assumptions. The effects of the assumptions regarding heat loss to the air and upstream heat conduction were examined by using finite element models. The Watronix inbM1-8-1.3-0.4 module was modeled in Solidworks in connection with a fluid-filled capillary and a muscle heat source far upstream ensuring the fluid temperature was constant across its cross-section when it reached the muscle. The exposed walls of the capillary and thermopile were adiabatic except for the bottom surface of the thermopile, which was held at a constant temperature. Consequently, heat was only lost via the fluid outflow and through the thermopile. The finite element model gave the expected temperature difference across the thermopile, which was then used to calculate the SNR as limited by Johnson noise.

The analytical model gave a SNR of 9540 for a single Watronix inbM1-8-1.3-0.4 thermopile. The finite element model with no upstream sensor or heat loss to the air predicted a SNR of 6410. The difference between this result and the analytical result likely reflects the effect of axial heat conduction through the fluid and the glass as well as variations in fluid temperature across its cross-section. The next model included an air layer similar to that occurring in the calorimeter, allowing heat to flow from the capillary to the housing. The resulting heat loss through the air decreased the SNR to 4910. Another model did not include the air layer but, instead, included the upstream thermopile located 4 mm away from the downstream thermopile. The muscle was located between the two thermopiles and a SNR of 3810 resulted. However, a large component of the reduction in SNR was due to the differential nature of measurement. Comparing the output of the modules causes no change in sensitivity but increases the noise by a factor of $\sqrt{2}$. Ignoring the increase in noise, the SNR is reduced to 5390 as a result of heat conduction to the upstream thermopile. Relaxing both assumptions, allowing heat loss through the air and with sensors upstream and downstream of the muscle, gives a SNR of 3530.

The thermopiles listed in table I were examined using finite element modeling, with the results shown in table II. The general trends are similar to the analytical predictions but have much smaller SNRs, partly due to the reasons discussed above. Additionally, size constraints impact the achievable SNR. For example, the analytical model predicted that the Laird

Module	Number of modules	Temperature Difference (mK)[a]	Predicted signal (µV)	Noise (nV)[b]	Analytic SNR	Finite Element Model SNR	Amplifier-limited SNR
Laird OT080203	1	1.49	1.20	0.30	9820	4000	140
	2	1.01	1.63	0.43	9680	3830	180
	3	0.74	1.79	0.52	9090	3440	200
Micropelt MPC-D303	1	0.26	0.21	0.22	6150	930	20
Micropelt MPG-D651	1	0.013	0.75	5.52	5160	140	30
Watronix inbM1-4-1.6-1.3	1	0.80	0.65	0.46	9560	2560	70
Watronix inbM1-8-1.3-0.4	1	1.53	2.47	0.70	9540	3530	260
	2	1.50	4.85	0.99	9880	4900	490
	3	1.19	5.78	1.21	9540	4770	570

a. Temperature difference was estimated with the muscle centered between the upstream and downstream modules with a flow rate of 0.5 µl/s and a heat output of 10 µW.
b. Predicted from Johnson noise over a 5 Hz bandwidth.

OT080203 would have a response between that of using one and two of the Watronix inbM1-8-1.3-0.4 modules. This was not observed using the finite element model. The probable cause of the reduced SNR of the Laird module was the size constraints on the measurement chamber. The Laird module was longer than the Watronix, so the upstream and downstream modules had to be closer together, resulting in more heat transfer to the upstream sensor.

In practice, the amplifiers used to measure the output of the thermopiles inject noise. Consequently, the amplifier-limited SNR must also be considered. Measurements were to be made using Keithley 2182A nanovoltmeters. These had an underlying noise of 6 nV which increases to 8 nV for a source resistance of 100 Ω. The SNR is dramatically reduced as a result but, once again, the Watronix inM1-8-1.3-0.4 module was predicted to have the highest SNR.

III. EXPERIMENTAL METHODS

Validation experiments were performed by constructing a microcalorimeter with one Laird OT080203 thermopile at each end. A gravity feed system was used to ensure a steady flow rate of 0.5 μl/s, measured using a mass balance (Mettler Toledo NewClassic MS). The thermopile output was measured using Keithley 2182A nanovoltmeters, which were polled at 10 Hz. The output of the mass balance and the nanovoltmeters were read via a USB/GPIB interface and processed using National Instruments LabVIEW.

The sensitivity was found by measuring the thermopile output in response to a known heat source. A 1 kΩ surface-mount resistor (0402 package) was used as the heat source and all applied electrical power was assumed to be dissipated as heat within the resistor. The resistor was attached to a 0.7 mm outer diameter borosilicate capillary and positioned in the center of the measurement chamber.

The noise was measured in the absence of any heat source. Ten 100 s long signals were recorded and their power spectral densities calculated. The resulting power spectral densities were averaged and the RMS magnitude of the resulting signal was calculated over a 5 Hz bandwidth to find the voltage noise.

IV. RESULTS AND CONCLUSIONS

The experimentally-determined sensitivity of the calorimeter was 0.149 V/W at a flow rate of 0.5 μl/s. The finite element model predicted a sensitivity of 0.120 V/W. The lower predicted sensitivity may be because the heat source is modeled as a muscle. The length of the muscle (as compared to the resistor) means it is in closer proximity to both the upstream and the downstream sensors. Heat conduction to the upstream sensor therefore may reduce the predicted temperature change. The analytical model, by comparison, predicted a sensitivity of 0.217 V/W.

Over a 5 Hz bandwidth the RMS magnitude of the noise power spectrum was 7.92 nV, which corresponds to 53 nW. The SNR for a 10 μW signal is therefore 190. This compares well with the amplifier-limited SNR of 140 predicted by the finite element model. The observed SNR is higher than that predicted by the model due to the lower predicted sensitivity

and the better-than-specified noise performance of the nanovoltmeter.

The resolution over a 1 Hz bandwidth was 24 nW. Focusing on maximizing the SNR rather than the sensitivity therefore has resulted in a two-fold increase in resolution over previous thermopile-based for heat balance calorimeters [11].

V. FUTURE WORK

The SNR was 190 at a flow rate of 0.5 μl/s over a 5 Hz bandwidth. The predicted SNR of the ABI calorimeter with these parameters is 140 [12]. Some improvement of the SNR was seen, further improvement could be achieved by using Watronix inbM1-8-1.3-0.4 modules. Using a single Watronix module could nearly double the SNR and by using three modules, a four-fold increase in SNR could result.

The SNR is primarily limited by noise from the measurement system rather than the inherent Johnson noise of the chips. In particular, the noise from the nanovoltmeters limited the obtainable resolution. The thermopiles considered have resistances on the order of one ohm, requiring matching instrumentation to fully realize the potential for reduced noise. Work is underway to implement a measurement system based on the EM Electronics model A10 amplifier, which is specified to 1.8 nV RMS noise for differential measurements under our experimental conditions. These should allow the SNR to be increased to 1300 using a single Watronix inbm1-8-1.3-0.4 module, or to 2700 with three of these modules.

REFERENCES

[1]   J. Steinbach, *Safety Assessment for Chemical Processes*. Weinheim, Germany: Wiley-VCH Verlag GmbH, 1998.

[2]   M. Meeks, "An analog computer study of polymerization rates in vinyl chloride suspensions," *Polym. Eng. Sci.*, no. 2, pp. 141–151, 1969.

[3]   A. Zogg, F. Stoessel, U. Fischer, and K. Hungerbühler, "Isothermal reaction calorimetry as a tool for kinetic analysis," *Thermochim. Acta*, vol. 419, no. 1–2, pp. 1–17, Sep. 2004.

[4]   J. Daut and G. Elzinga, "Heat Production of Quiescent Ventricular Trabeculae Isolated from Guinea-Pig Heart," *J. Physiol.*, vol. 398, no. 1988, pp. 259–275, 1988.

[5]   K. Lee, "A new technique for the simultaneous recording of oxygen consumption and contraction of muscle: the effect of ouabain on cat papillary muscle," *J. Pharmacol. Exp. Ther.*, pp. 304–312, 1953.

[6]   J.-C. Han, A. J. Taberner, R. S. Kirton, P. M. F. Nielsen, R. Archer, N. Kim, and D. S. Loiselle, "Radius-dependent decline of performance in isolated cardiac muscle does not reflect inadequacy of diffusive oxygen supply," *Am. J. Physiol. - Hear. Circ. Physiol.*, pp. 1222–1236, 2011.

[7]   J.-C. Han, A. J. Taberner, R. S. Kirton, P. M. F. Nielsen, N. P. Smith, and D. S. Loiselle, "A unique micromechanocalorimeter for simultaneous measurement of heat rate and force production of cardiac trabeculae carnae," *J. Appl. Physiol.*, vol. 107, pp. 946–951, 2009.

[8] M. Zieren, R. Willnauer, and J. Köhler, "Flow-through chip calorimeter based on BiSb/Sb-thin-film thermopiles with a thermopower of 64 mV/K," *Micro Total Anal. Syst. 2000*, no. 100, pp. 71–74, 2000.

[9] A. W. van Herwaarden, P. M. Sarro, J. W. Gardner, and P. Bataillard, "Liquid and gas micro-calorimeters for (bio)chemical measurements," *Sensors Actuators A Phys.*, vol. 43, no. 1–3, pp. 24–30, May 1994.

[10] V. Baier, A. Ihring, E. Kessler, J. Lerchner, and G. Wolf, "Highly sensitive thermopile heat power sensor for micro-fluid calorimetry of biochemical processes," *Sensors Actuators A Phys.*, vol. 123–124, pp. 354–359, Sep. 2005.

[11] J. Lerchner, a. Wolf, G. Wolf, V. Baier, E. Kessler, M. Nietzsch, and M. Krügel, "A new micro-fluid chip calorimeter for biochemical applications," *Thermochim. Acta*, vol. 445, no. 2, pp. 144–150, Jun. 2006.

[12] A. J. Taberner, I. W. Hunter, R. S. Kirton, P. M. F. Nielsen, and D. S. Loiselle, "Characterization of a flow-through microcalorimeter for measuring the heat production of cardiac trabeculae," *Rev. Sci. Instrum.*, vol. 76, no. 10, pp. 104902–7, Oct. 2005.

[13] J. H. Lienhard IV and J. H. Lienhard V, *A heat transfer textbook*, 4th ed., vol. 27, no. 4. Cambridge, MA: Phlogiston Press, 2011.

[14] M. C. Foote, E. W. Jones, and T. Caillat, "Uncooled thermopile infrared detector linear arrays with detectivity greater than 10^9 cmHz$^{1/2}$/W," *IEEE Trans. Electron Devices*, vol. 45, no. 9, pp. 1896–1902, 1998.

[15] B. Yang, H. Ahuja, and T. Tran, "Review Article: Thermoelectric Technology Assessment: Application to Air Conditioning and Refrigeration," *HVAC&R Res.*, no. January 2014, pp. 37–41, 2008.

[16] H. Kraus, "Superconductive bolometers and calorimeters," *Supercond. Sci. Technol.*, vol. 9, no. 10, pp. 827–842, Oct. 1996.

[17] W. Franzen, "Nonisothermal Superconducting Bolometer: Theory of Operation," *J. Opt. Soc. Am.*, vol. 53, no. 5, p. 596, May 1963.